



Trans. Nonferrous Met. Soc. China 27(2017) 2291-2299

Transactions of Nonferrous Metals Society of China

www.tnmsc.cn



# Nucleation/growth mechanism of electrocrystallization for As-Sb alloy in hydrochloric acid system

Hua-zhen CAO, Yu-feng ZHANG, Qian-qian WANG, Lian-kui WU, Guo-qu ZHENG
College of Materials Science and Engineering, Zhejiang University of Technology, Hangzhou 310014, China
Received 17 June 2016; accepted 23 November 2016

**Abstract:** The initial electrocrystallization of As–Sb alloy on glass carbon (GC) electrode in hydrochloric acid system was studied via cyclic voltammetry (CV) and chronoamperometry measurements. Current transients were presented in dimensionless formation, which showed that the initial nucleation/growth process of As–Sb alloy followed three-dimensional nucleation model with diffusion-controlled growth. Relevant nucleation parameters were calculated by analyzing related current transients. Particular attention was paid to the effect of Sb(III) concentration on the nucleation process during the co-electrodeposition. The quantitative results showed that Sb(III) played a positive effect on enhancing the nucleation rate of As–Sb alloy, leading to the evolution of alloy surface morphology from grain structure to compact layer structure.

**Key words:** arsenic; antimony; As–Sb alloy; electrodeposition; nucleation

# 1 Introduction

The contamination of arsenic compounds from waste disposals is a worldwide problem and has become a challenge for both academic and industrial communities. To solve this problem, scientists have proposed many treatment strategies, aiming to efficiently remove, recycle, and utilize the waste arsenic. For the removal of arsenic, some technologies including chemical precipitation [1], ion exchange [2], membrane separation [3] and adsorption [4] have been developed, which can effectively remove the arsenic from waste or contaminated water. However, large amount of arsenic-bearing compounds are produced, which become secondary contamination. The electrodeposition of elemental arsenic seems to be a good way to obtain nontoxic and valuable material. Despite many efforts devoted to this method, there still remain some difficulties in terms of arsine evolving and low current efficiency [5–9]. Recently, increasing attention has been paid to the co-deposition of arsenic with other metals [10-14] to prepare functional alloy, by which the evolution of arsine could be efficiently inhibited and the current efficiency was obviously enhanced [15]. Among these functional alloys, As-Sb alloy and As-Sbbased alloy have a broad prospect in photoelectric conversion [16], semiconductor [17,18] and thermomagnetic devices [19,20]. Therefore, the study of electrodeposition of As–Sb alloy is meaningful. Besides, the standard electrode potential of Sb(III)–(0) is close to that of As(III)–(0), which indicates that the co-deposition of arsenic with antimony from their aqueous solutions is easy and feasible.

In the past years, we have made many efforts in electrodeposition technology and process of As-Sb alloy [15,21], and could continuously electrolyze for 8 h or longer time. The prepared As-Sb alloy showed typical metallic luster with current efficiency higher than 90% and the mass fraction of As in deposits ranging from 30% to 70%. However, a fundamental study such as nucleation and growth mechanism is insufficient. For alloys, the quality and property of alloy are usually determined by their composition and microstructure. For example, the band gap energy of In-As thin films shows strong dependence on the crystalline size [22], as another example, some alloys with finer grains provide superior corrosion resistance [23]. For metal electrodeposition, the formation of alloy consists of two processes: 1) the nucleation which induces the embryo of crystalline, and 2) the growth of the crystalline. Generally, nucleation plays a more important role in determining the microstructure of alloy. High nucleation rate usually leads to fine grains. Therefore, it is of great importance to investigate the nucleation and initial electrocrystallization process in electrodeposition. Potentiostatic current transient is an efficient electrochemical method to investigate the kinetics of nucleation. By applying typical models which describe the early stages of electrocrystallization [24–28], the mechanisms of electrochemical nucleation and crystal growth in different circumstances can be revealed.

In this work, CV method and chronoamperometry technique were used to investigate the initial behavior of As–Sb alloy during electrocrystallization process and reveal its nucleation/growth mechanism. Specifically, the influences of Sb(III) concentration on the nucleation rate and grain size were investigated in detail combined with scanning electron microscopy (SEM) observation.

# 2 Experimental

Electrolytes used in experiments contained 0-15 g/L As(III), 0-20 g/L Sb(III) and 2 mol/Lhydrochloric acid, which were freshly prepared with purified AsCl<sub>3</sub> and SbCl<sub>3</sub> aqueous solutions generated from the treatment of lead anode slime [29,30]. CV and potentiostatic transient curves were measured to investigate the initial electrocrystallization mechanisms of As-Sb alloy. All electrochemical tests were carried out at room temperature on CHI660C electrochemical workstation in a three electrode cell. A GC electrode with surface area of 0.1256 cm<sup>2</sup> was used as the working electrode. A saturated calomel reference electrode (SCE) was served as the reference electrode and a Pt slice was used as the counter electrode. Prior to experiments, GC electrode was polished and thoroughly rinsed by deionized water. Before each experiment, high purity nitrogen was bubbled into the system to eliminate the dissolved oxygen.

Electrodeposition was carried out under constant current density of 2 mA/cm² for 10 min. The morphology of the deposit was observed by scanning electron microscopy (SEM, VEGA3). The chemical composition of the deposit was determined by X-ray fluorescence (XRF, ThermoFisher/ARLADVANT'X IntelliPowerTM 4200). The phase composition of the deposit was also characterized by employing X-ray diffraction (XRD, RIGAKU D/Max 2550 PC).

# 3 Results and discussion

### 3.1 Cyclic voltammetry study

The main reactions occurred during electrodeposition were first determined by CV measurements. Figure 1(a) presents the CV curves of As electrodeposition from solutions with 2 mol/L HCl and different concentrations of As(III) on a GC electrode. For comparison, the CV curve for blank solution only containing 2 mol/L HCl is also presented. It can be observed that a broad and weak cathodic peak  $(P_0)$ occurs at about -0.48 V for blank solution, after that the cathodic current tends to increase monotonously. The reduction current arising in this case is associated with the adsorption of intermediate H on GC electrode [31–33]. For As(III)-containing solutions, it can be found that in the negative potential sweep, the reduction of As(III) begins at a potential of -0.1 V, after that the cathodic current increases and two current peaks emerge at potential of  $-0.31 \text{ V}(P_1)$  and  $-0.51 \text{ V}(P_2)$ , respectively. In prior studies [5-9,15,34,35], it has been confirmed that the As deposition is often accompanied with the evolution of arsine, and the formation of arsine is closely related to the reduction of H<sup>+</sup>. As can be seen that the potential of  $P_2$  is very close to that of  $P_0$ , so it is obvious that the  $P_2$  is related to the evolution of arsine and the  $P_1$  denotes the reduction of As(III) to As. However, the cathodic current is low albeit it increases as As(III) concentration changes from 5 to 15 g/L, which is due to the non-conductivity of electrodeposited arsenic [5,6,36].

CV curves of Sb electrodeposition from solutions with 2 mol/L HCl and different concentrations of Sb(III) on GC electrode are shown in Fig. 1(b). An obvious cathodic peak ( $P_3$ ) is observed at about -0.29 V, which corresponds to the reduction of Sb(III) to Sb. For the reverse scanning, a current loop appears between anodic and cathodic current curves. The presence of this current loop is a typical characteristic representing the nuclei formation of metal antimony on electrode [37,38]. Furthermore, it is clear that the current peak becomes stronger with the increase of Sb(III) concentration, which suggests that the reduction process is facilitated by the higher Sb(III) concentration.

Following the individual electrodeposition of As(III) and Sb(III), their CV curves were carried out in the solutions with various concentrations of As(III) and Sb(III) (Figs. 1(c) and (d)), respectively. For all curves, two cathodic peaks ( $P_4$  and  $P_5$ ) are observed. The peak  $P_4$  (-0.28 V), which shows a slight shift as compared with that (-0.29 V) from pristine Sb deposition, becomes stronger with the increase of Sb(III) concentration while is less affected by the As(III) concentration. So it can be confirmed that the  $P_4$  is related to the reduction of Sb(III). Being different from  $P_4$ , the  $P_5$  emerges at more negative potential than  $P_4$  and is close to the peak  $P_1$  of As(III) reduction. However, the current value is much higher that obtained in the individual As(III) electrodeposition. It may be speculated that the strong peak  $P_5$  corresponds to the reduction of As(III) and

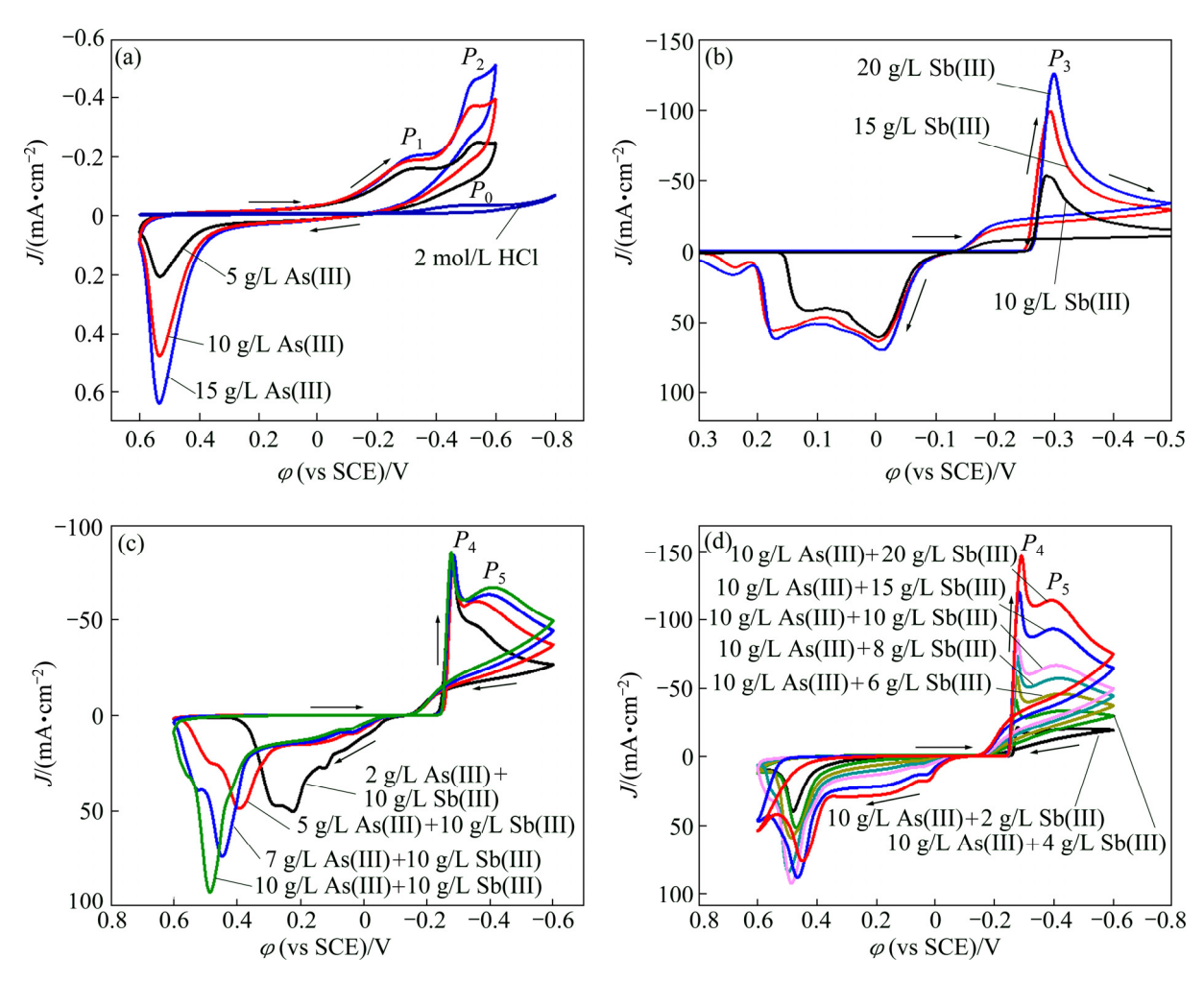
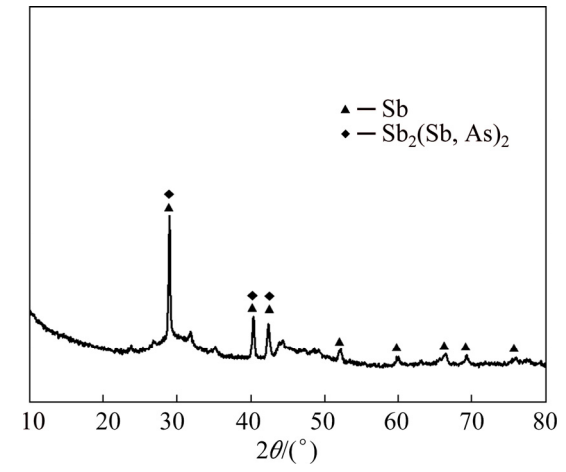


Fig. 1 Cyclic voltammograms of GC in solutions containing various As(III) concentrations (a), various Sb(III) concentrations (b), 10 g/L Sb(III) and various As(III) concentrations (c), and 10 g/L As(III) and various Sb(III) concentrations (d) at scan rate of 50 mV/s

Sb(III) to form As–Sb alloy. In addition, the cathodic current is enhanced monotonously with increasing the Sb(III) concentration, indicating that Sb(III) has a significant stimulative effect on the deposition of alloy. Similarly, crossover between anodic and cathodic current curves also appears on the reverse potential sweep, denoting the nuclei formation of As–Sb alloy.

### 3.2 XRD and XRF analysis

The compositions of cathodic deposits were characterized by XRD to verify the inferences mentioned in the above CV study. The diffraction pattern of deposits from solutions containing 10 g/L As(III) and 6 g/L Sb(III) are exhibited in Fig. 2. According to the Joint Diffraction Committee Powder Standards on (00-001-0802) and (00-025-0048), the diffraction peaks of Sb and Sb<sub>2</sub>(Sb, As)<sub>2</sub> are overlapped in  $2\theta$  range of  $29.0^{\circ}$  –  $42.4^{\circ}$ , and the weak peaks at  $2\theta$  of  $52.1^{\circ}$ ,  $59.9^{\circ}$ , 66.3°, 69.3° and 76.0° prove the existence of Sb. With the aid of XRF (Table 1), it reveals that the cathodic product is composed of large number of arsenic and



**Fig. 2** XRD pattern of deposits prepared under constant current density of 2 mA/cm<sup>2</sup> for 10 min from solutions containing 2 mol/L HCl, 10 g/L As(III) and 6 g/L Sb(III)

antimony. XRD and XRF analyses confirm that the codeposition of As and Sb from As(III)-Sb(III)-HCl system can be achieved under certain experiment condition.

**Table 1** Mass ratio of As to Sb in deposits prepared under constant current density of 2 mA/cm<sup>2</sup> for 10 min from solutions containing 2 mol/L HCl, 10 g/L As(III) and various concentrations of Sb(III)

Sb(III) concentration/(g·L <sup>-1</sup> )	Mass ratio of As to Sb in deposit
4	1:2.92
6	1:3
8	1:3.32
10	1:3.35

### 3.3 Potentiostatic study

# 3.3.1 Initial electrocrystallization process of As-Sb alloy

Chronoamperometry technique was applied to studying the nucleation and subsequent crystalline growth during the electrodeposition. For the purpose of determining the control process during the co-deposition of As–Sb alloy, CV curves with different scan rates were obtained from solutions containing 2 mol/L HCl, 10 g/L As(III) and 2 g/L Sb(III) firstly as shown in Fig. 3(a). Furthermore, a plot of peak  $(P_5)$  current density (J) versus the square root of scan rate  $(v^{1/2})$  was then obtained and shown in Fig. 3(b). It can be seen that the

current density J shows a good linear relation with  $v^{1/2}$ , which reveals that the deposition process of As–Sb alloy belongs to diffusion-controlled growth.

Figure 4(a) shows the transient current density obtained between -0.36 and -0.41 V from solutions containing 2 mol/L HCl, 10 g/L As(III) and 6 g/L Sb(III). The applied potential is carefully chosen in the broad range of peak P<sub>5</sub> where the co-deposition of As and Sb happens based on the CV study. More importantly, our previous study [15] has revealed that Sb can effectively inhibit the evolution of arsine during electrochemical co-deposition of As and Sb, which means that the evolution of arsine can also be negligible in such a condition. All curves perform a rising part followed by a maximum current density  $(J_m)$  at the initial stage, after that, the current density begins to decay and then reaches stability gradually. It can be seen that with the negative shift of applied potential, the value of  $J_{\rm m}$  increases gradually and the time to reach  $J_{\mathrm{m}}$  ( $t_{\mathrm{m}}$ ) shortens correspondingly. This suggests that the cathodic shift of applied potential accelerates the nucleation and decreases the nucleation induction time.

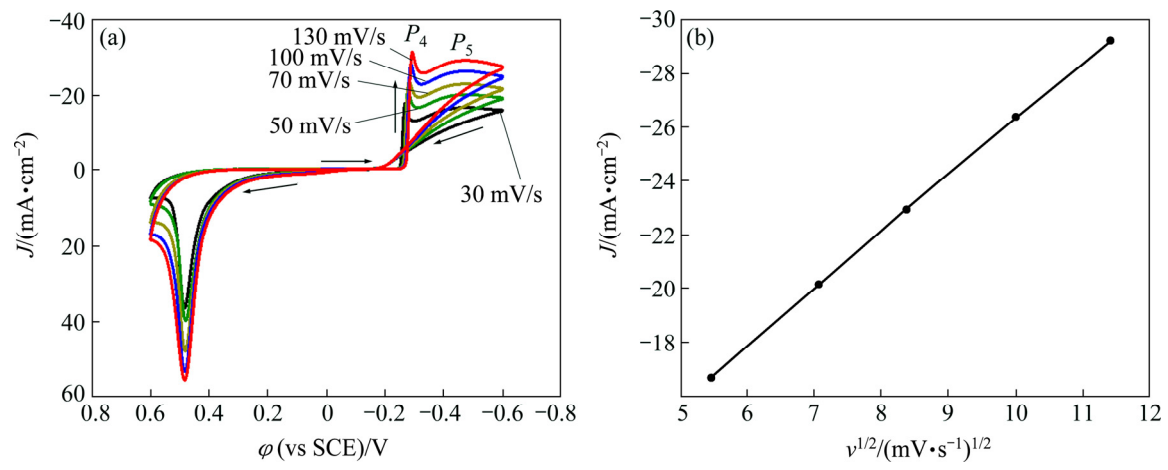


**Fig. 3** Cyclic voltammograms of GC in solutions containing 2 mol/L HCl, 10 g/L As(III) and 2 g/L Sb(III) at scan rates of 30, 50, 70, 100 and 130 mV/s (a) and plot of peak ( $P_5$ ) current density J vs square root of scan rate  $v^{1/2}$  (b)

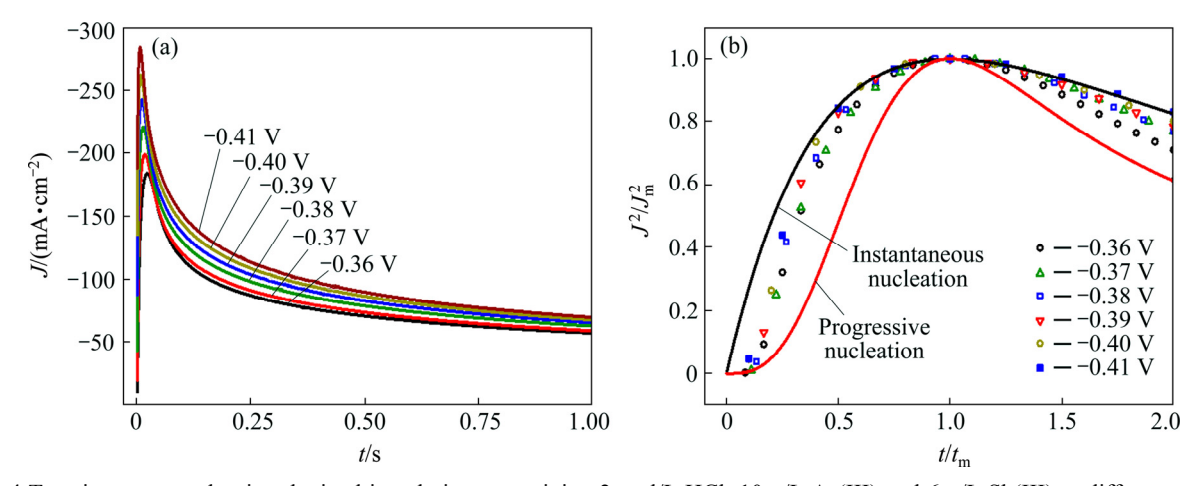


Fig. 4 Transient current density obtained in solutions containing 2 mol/L HCl, 10 g/L As(III) and 6 g/L Sb(III) at different applied potentials (a), and comparison of experimental 3D dimensionless nucleation curves with theoretical 3D nucleation plots (b)

Several nucleation/growth models have been proposed to explain the electrochemical processes including the generation of new phase [24–26,28]. In the case of the co-deposition of As and Sb, the transient curves exhibit a typical feature of 3D nucleation process [39] as proposed by SCHARIFKER et al [24,25]. This 3D nucleation model has two extreme cases and the correlative equations are as follows:

$$J^{2}/J_{\rm m}^{2} = \frac{1.9542}{t/t_{\rm m}} \left\{ 1 - \exp[-1.2564(t/t_{\rm m})] \right\}^{2}$$
 (1)

$$J^{2}/J_{\rm m}^{2} = \frac{1.2254}{t/t_{\rm m}} \{1 - \exp[-2.3367(t^{2}/t_{\rm m}^{2})]\}^{2}$$
 (2)

where J represents the current density, t represents the time,  $J_{\rm m}$  represents the maximum current density and  $t_{\rm m}$  is the time corresponding to  $J_{\rm m}$ . Equation (1) represents the instantaneous nucleation condition with extremely faster growth rate and fewer active nucleation sites, while Eq. (2) represents the progressive nucleation condition with slower growth rate but larger numbers of active nucleation sites. The nucleation growth mechanism can be determined by comparing the experimental plots with theoretical nucleation plots derived from Eqs. (1) and (2).

Figure 4(b) gives a comparison of experimental plots obtained at different applied potentials from solution containing 2 mol/L HCl, 10 g/L As(III) and 6 g/L Sb(III) with the theoretical 3D dimensionless plots derived from Eqs. (1) and (2). It can be seen that all of the experimental plots obtained from -0.36 to -0.41 V fall between the theoretical instantaneous nucleation curve and progressive nucleation curve, which suggests that the nucleation/growth mechanism of As-Sb alloy follows 3D nucleation model with diffusion control. It is noted that with the negative shift of applied potential, experimental curve becomes broader and draws nearer to the theoretical instantaneous nucleation curve gradually. In other words, nucleation rate increases with the negative shift of applied potential.

From the CV results concluded from Fig. 1(d), we got to know that Sb(III) has a significant stimulative effect on the deposition of As–Sb alloy. For the further understanding of the effect of Sb(III), a series of electrochemical measurements were carried out in the solutions containing 2 mol/L HCl, 10 g/L As(III) and varied concentrations of Sb(III). Figure 5 shows the comparison of relevant experimental nucleation curves obtained under –0.36 V with the theoretical 3D nucleation plots. It is clear that with the gradual increase of Sb(III) concentration, experimental nucleation curve widens and approaches the theoretical instantaneous nucleation plot, meaning that the nucleation rate

increases at higher Sb(III) concentration. This phenomenon also proves that Sb(III) could accelerate the nucleation/growth rate of As–Sb alloy.

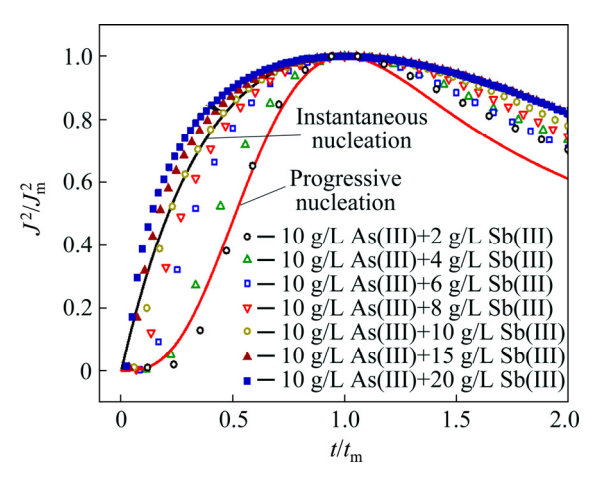


**Fig. 5** Experimental 3D dimensionless nucleation curves obtained from solutions containing 2 mol/L HCl, 10 g/L As(III) and various Sb(III) concentrations at -0.36 V with theoretical 3D nucleation plots

### 3.3.2 Quantitative analysis of nucleation process

Based on the above discussion, we have demonstrated that the nucleation/growth process of As–Sb alloy follows 3D nucleation with diffusion controlled growth. Relevant kinetics parameters during electrocrystallization process were calculated by analyzing the increasing portion of transients current density as well as the maximum current density ( $J_{\rm m}$ ) and time ( $t_{\rm m}$ ). SCHARIFKER and MOSTANY [24] have proposed the relationship between current density and time with consideration of hemispherical diffusion into the growing crystallites, the equation is as follows:

$$J = [zFD^{1/2}c/(\pi^{1/2}t^{1/2})]\{1 - \exp[-N_0\pi kD \cdot (t - (1 - \exp(-At))/A)]\}$$
(3)

where z represents the number of electrons, F is the Faraday constant, D is the diffusion coefficient, c is the concentration of active species in the bulk,  $N_0$  is the number density of active sites and A represents the nucleation rate per active site.

Recently, DÍAZ-MORALES et al [28] have developed this model for the calculation of nucleation/growth kinetic parameters of bimetallic by considering the binary components as one pseudo component. The expression of the nucleation/growth of bimetallic phases is analogous to Eq. (3), as the following Eq. (4) shows:

$$J = [-D_{w}Fc^{*}/(\pi^{1/2}D_{a}^{1/2}t^{1/2})] \cdot$$

$$\{1 - \exp[-N_{0}\pi kD_{a}^{1/2}D_{w}^{1/2}(t - (1 - \exp(-At))/A)]\}$$
 (4)

where  $c^*$  corresponds to the bulk concentration of the

pseudo-ion,  $D_{\rm w}$  and  $D_{\rm a}$  represent the mass and charge coefficient and apparent diffusion coefficient, respectively, k is the dimensionless constant that affects the growth rate of diffusion zones. The values of  $c^*$ ,  $D_{\rm w}$ ,  $D_{\rm a}$  and k can be determined by calculating sequential equations as follows:

$$c^* = c_1^* = \gamma c_2^* \tag{5}$$

$$D_{w} = (z_{1}D_{1}\gamma + z_{2}D_{2})/[(\gamma(z_{1}x_{1} + z_{2}x_{2}))]$$
 (6)

$$D_{a} = (D_{1}\gamma + D_{2})/(\gamma + 1) \tag{7}$$

$$k = \sqrt{8\pi c^* (x_1 v_{m,1} + x_2 v_{m,2})}$$
 (8)

where  $c_1^*$  and  $c_2^*$  refer to the bulk concentrations of the two component species,  $\gamma$  equals to  $c_1^*/c_2^*$ ,  $x_1$  equals  $c_1^*/(c_1^*+c_2^*)$  and  $x_2$  equals  $c_2^*/(c_1^*+c_2^*)$ ,  $z_1$  and  $z_2$  are the electron numbers of the two component species, with  $D_1$  and  $D_2$  corresponding to the diffusion coefficient of As(III) and Sb(III) in the solutions and  $v_{\rm m,1}$ , and  $v_{\rm m,2}$  denote the moral volumes, respectively. By dealing Eq. (4) with derivative operations and making substitution of x for  $N_0\pi k D_{\rm a}^{1/2} D_{\rm w}^{1/2} t_{\rm m}$ ,  $\alpha$  for  $N_0\pi k D_{\rm a}^{1/2} D_{\rm w}^{1/2} /A$  and  $\alpha$  for  $D_{\rm w} F c^*/(\pi^{1/2} D_{\rm a}^{1/2})$ , Eqs. (9) and (10) can be obtained as follows:

$$In[1 + 2x(1 - \exp(-x/\alpha))] - x + \alpha(1 - \exp(-x/\alpha)) = 0$$
 (9)

$$\ln(1 - J_{\rm m} t_{\rm m}^{1/2} / a) + x - \alpha (1 - \exp(-x/\alpha)) = 0$$
 (10)

There are three unknown variables in Eqs. (9) and (10). If we assume the value of  $\alpha$ , then the other two unknown variables, i.e., x and a, can be calculated. Meanwhile, an equation describing the relationship of diffusion coefficient  $D_1$  and  $D_2$  of the electrochemical active ions can be constructed based on the Cottrell equation:

$$\frac{J_1}{J_2} = \frac{z_1 F D_1^{1/2} c_1 / (\pi^{1/2} t^{1/2})}{z_2 F D_2^{1/2} c_2 / (\pi^{1/2} t^{1/2})}$$
(11)

By XRF analysis, the mass ratios of As to Sb in deposits were obtained (Table 1), from which the ratio of  $J_1/J_2$  was determined. Combining  $\alpha$ , x, a, and Eqs. (6)–(8) and (11), the values of  $D_1, D_2, D_a, D_w, A$  and  $N_0$  are obtained. According to the calculated  $D_a, D_w, A$ ,  $N_0$  and Eq. (4), we can get a calculated current density—time curve. Figure 6 shows a series of non-dimensional plots derived from the calculated current density—time curves at different hypothetical values of  $\alpha$  from

solutions containing 2 mol/L HCl, 10 g/L As(III) and 6 g/L Sb(III). It is found that the peak of dimensionless plot becomes sharper with the increase of  $\alpha$ , and the calculated plot at  $\alpha$ =0.17 fits quite well with the experimental plot in the range of  $t/t_{\rm m}$ <1, which indicates that this value of  $\alpha$  for fitting is reliable. Then, the values of  $D_{\rm As(III)}$ ,  $D_{\rm Sb(III)}$ ,  $D_{\rm a}$ ,  $D_{\rm w}$ , A and  $N_0$  are determined as  $1.91\times10^{-6}$  cm<sup>2</sup>/s,  $4.74\times10^{-5}$  cm<sup>2</sup>/s,  $1.42\times10^{-5}$  cm<sup>2</sup>/s,  $1.95\times10^{-5}$  cm<sup>2</sup>/s, 394.5 s<sup>-1</sup> and  $5.83\times10^{5}$  cm<sup>-2</sup>, respectively. However, derivation appears at extending time, which may be due to the hydrogen evolution on the deposited nuclei or the change of morphology from hypothesis hemispherical geometry [40,41], and the latter explanation seems more possible under this condition.

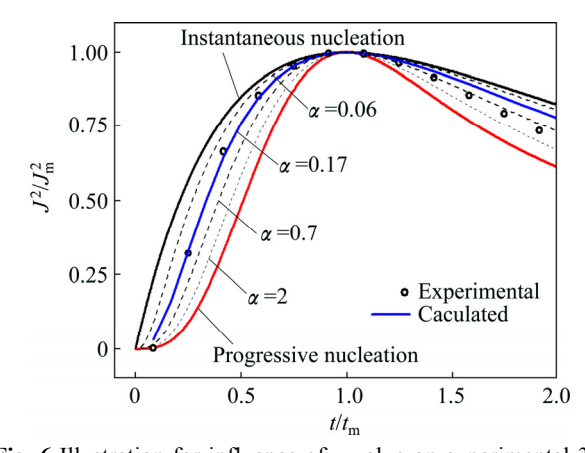


**Fig. 6** Illustration for influence of  $\alpha$  value on experimental 3D dimensionless nucleation plots obtained from solution containing 2 mol/L HCl, 10 g/L As(III) and 6 g/L Sb(III) at -0.36 V

Table 2 presents the calculated results of the experimental curves obtained from solutions containing 2 mol/L HCl, 10 g/L As(III) and various concentrations of Sb(III). The variations of A and  $N_0$  with the gradual increase of Sb(III) concentration are exhibited in Figs. 7(a) and (b), respectively. It is found that with increasing the concentration of Sb(III) in the solutions, nucleation rate A increases while number density of active nucleation sites  $N_0$  decreases. In addition, the value of A increases rapidly when Sb(III) concentration varies from 8 to 10 g/L, which can be due to the fact that the experimental nucleation curve almost overlaps with the theoretical instantaneous nucleation plot under such a condition, implying a fast nucleation rate.

**Table 2** Calculated values for  $D_{As(III)}$ ,  $D_{Sb(III)}$ ,  $N_0$  and A at various Sb(III) concentrations

Sb(III) concentration/(g·L <sup>-1</sup> )	$\varphi/{ m V}$	$t_{\rm m}/{\rm s}$	$J_{\mathrm{m}}/(\mathrm{mA\cdot cm}^{-2})$	$D_{\mathrm{As(III)}}/(\mathrm{cm}^2\cdot\mathrm{s}^{-1})$	$D_{\mathrm{Sb(III)}}/(\mathrm{cm}^2\cdot\mathrm{s}^{-1})$	$N_0/\mathrm{cm}^{-2}$	$A/s^{-1}$
4	-0.36	0.018	145.2	$0.56 \times 10^{-6}$	$2.97 \times 10^{-5}$	$39.90 \times 10^6$	107.3
6	-0.36	0.024	184.2	$1.91 \times 10^{-6}$	$4.74 \times 10^{-5}$	$5.83 \times 10^{6}$	394.5
8	-0.36	0.030	210.7	$3.31 \times 10^{-6}$	$5.63 \times 10^{-5}$	$2.63 \times 10^{6}$	671.7
10	-0.36	0.035	240.0	$5.81 \times 10^{-6}$	$6.51 \times 10^{-5}$	$1.44 \times 10^6$	3655.6

#### 3.3.3 SEM observation

Figure 8 shows the SEM images of deposits prepared from solutions containing 2 mol/L HCl, 10 g/L As(III) and different concentrations of Sb(III), and single

arsenic deposits are also observed for comparison. For arsenic deposits, lots of irregular grains are loosely distributed on the surface. However, with the introduction of Sb(III) into the arsenic solution, the

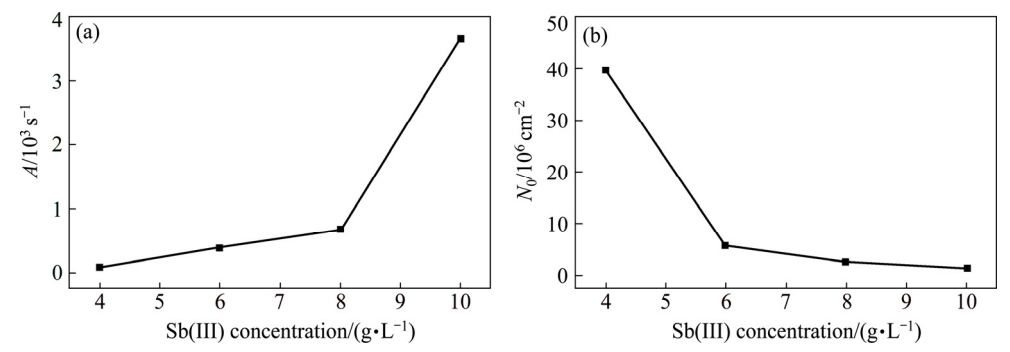
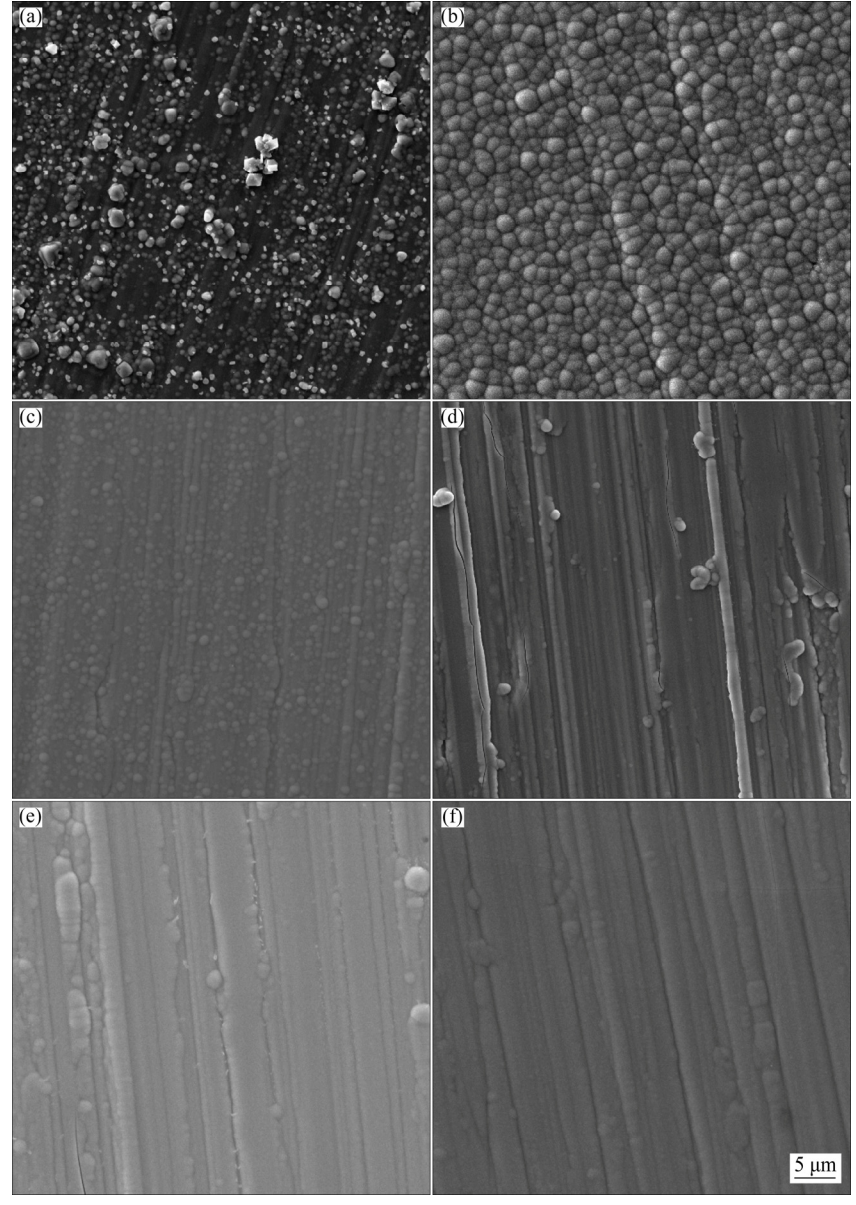


Fig. 7 Influence of Sb(III) concentration on nucleation rate A (a) and number density of active sites  $N_0$  (b)



**Fig. 8** Surface micro-morphologies of deposits prepared at constant current density of 2 mA/cm<sup>2</sup> for 10 min from solutions containing 2 mol/L HCl, 10 g/L As(III) and different Sb(III) concentrations: (a) Without Sb(III); (b) 2 g/L Sb(III); (c) 4 g/L Sb(III); (d) 6 g/L Sb(III); (e) 8 g/L Sb(III); (f) 10 g/L Sb(III)

deposits (Fig. 8(b)) present a more compact structure, in which the grains with uniform size regularly grow on the surface. It is obvious that the amount of deposits is significantly increased as compared with that of the single arsenic deposits under the similar electrodeposition conditions.

By gradually increasing the concentration of Sb(III), the evolution of surface morphology of the alloys was studied, as shown in Figs. 8(c)–(f). The microstructure of electrodeposits highly depends on the Sb(III) concentration in solution. When the Sb(III) concentration is lower than 6 g/L, surfaces are covered with compact grains, and specifically, the average size of grains decreases as increasing the Sb(III) concentration (Figs. 8(b) and (c)). In the cases of Sb(III) concentration higher than 6 g/L, no obvious grain structure is observed, instead, uniform and compact alloy layers are formed. The refined crystalline structure is likely caused by the high nucleation rate. The evolution of microstructure of the alloys further proves the facilitated effect of Sb(III) on the co-electrodeposition.

# **4 Conclusions**

- 1) Cyclic voltammetry study indicates that the addition of Sb(III) can facilitate the eletrodeposition process and As-Sb alloy can be prepared under optimal conditions. In addition, deposition process of As-Sb alloy belongs to diffusion controlled growth.
- 2) The chronoamperometry study reveals that initial nucleation/growth mechanism of As-Sb alloy follows 3D nucleation model. Quantitative analyses of initial nucleation process give the values of nucleation rate and number of active nucleation sites at various Sb(III) concentrations. Nucleation rate increases by the addition of Sb(III).
- 3) The microstructure of electrodeposits is proved to be highly dependent on the Sb(III) concentration. Irregular grains will grow on the surface in the absence of Sb(III), while the addition of Sb(III) will lead to form regular grains. The grain size of deposits decreases with the increase of Sb(III) concentration, which finally brings about a uniform and compact structure.

### References

- TONGAMP W, TAKASAKI Y, SHIBAYAMA A. Precipitation of arsenic as Na<sub>3</sub>AsS<sub>4</sub> from Cu<sub>3</sub>AsS<sub>4</sub>-NaHS-NaOH leach solutions [J]. Hydrometallurgy, 2010, 105(1-2): 42-46.
- [2] SHAO Wen-jing, LI Xiao-min, CAO Qi-lin, LUO Fang, LI Jian-mei, DU Yang-yang. Adsorption of arsenate and arsenite anions from aqueous medium by using metal(III)-loaded amberlite resins [J]. Hydrometallurgy, 2008, 91(1-4): 138-143.
- [3] NGUYEN C M, BANG S, CHO J, KIM K W. Performance and mechanism of arsenic removal from water by a nanofiltration membrane [J]. Desalination, 2009, 245(1–3): 82–94.

- [4] GILES D E, MOHAPATRA M, ISSA T B, ANAND S, SINGH P. Iron and aluminum based adsorption strategies for removing arsenic from water [J]. Journal of Environmental Management, 2011, 92(12): 3011–3022.
- [5] BISANG J M, BOGADO F, RIVERA M O, DORBESSAN O L. Electrochemical removal of arsenic from technical grade phosphoric acid [J]. Journal of Applied Electrochemistry, 2004, 34(4): 375–381.
- [6] BRUSCIOTTI F, DUBY P. Co-deposition of arsenic and arsine on Pt, Cu, and Fe electrodes [J]. Electrochemistry Communications, 2008, 10(4): 572–576.
- [7] SMIRNOV M K, TURYGIN V V, SHALASHOVA N N, KHUDENKO A V, TOMILOV A P. Electrochemical reduction of As(III) in acid media [J]. Inorganic Materials, 2007, 43(1): 25–29.
- [8] DING W W, STURGEON R E. Interference of copper and nickel on electrochemical hydride generation [J]. Journal of Analytical Atomic Spectrometry, 1996, 11: 421–425.
- [9] BRUSCIOTTI F, DUBY P. Cyclic voltammetry study of arsenic in acidic solutions [J]. Electrochimica Acta, 2007, 52(24): 6644-6649.
- [10] CATTARIN S, MUSIANI M M, CASELLATO U, GUERRIERO P, BERTONCELLO R. Cathodic deposition of ternary In+As+Sb alloys and formation of InAs<sub>x</sub>Sb<sub>1-x</sub> [J]. Journal of Electroanalytical Chemistry, 1995, 380(1–2): 209–218.
- [11] MENGOLI G, MUSIANI M M, PAOLUCCI F. Synthesis of InAs and InAs<sub>1-x</sub>Sb<sub>x</sub> from electrodeposited layers of Indium, arsenic and As-Sb Alloy [J]. Journal of Electroanalytical Chemistry, 1992, 332(1-2): 199-211.
- [12] NAYAK J, SAHU S N. Effect of synthesis temperature on the structure and optical properties of electro-chemically grown GaAs nanocrystals [J]. Physica E: Low-dimensional Systems and Nanostructures, 2008, 41(1): 92–95.
- [13] VILLEGAS I, STICKNEY J L. Preliminary studies of GaAs deposition on Au(100), (110), and (111) surfaces by electrochemical atomic layer epitaxy [J]. Journal of the Electrochemical Society, 1992, 139(3): 686–694.
- [14] WADE T L, VAIDYANATHAN R, HAPPEK U, STICKNEY J L. Electrochemical formation of a III–V compound semiconductor superlattice: InAs/InSb [J]. Journal of Electroanalytical Chemistry, 2001, 500(1–2): 322–332.
- [15] SHAN Hai-peng, CAO Hua-zhen, ZHANG Yu-feng, RUAN Hui-min, ZHENG Guo-qu. Inhibitory effect of antimony on the evolution of arsine during electrochemical co-deposition of arsenic with antimony [J]. Journal of the Electrochemical Society, 2013, 160(10): E121-E124.
- [16] BELABBES A, ZAOUI A, FERHAT M. Alloying effect in the III-As-Sb ternary systems [J]. Materials Science and Engineering B, 2007, 137(1-3): 210-212.
- [17] HE J, REYNER C J, LIANG B L, NUNNA K, HUFFAKER D L. Band alignment tailoring of InAs<sub>1-x</sub>Sb<sub>x</sub>/GaAs quantum dots: Control of Type I to Type II transition [J]. Nano Letters, 2010, 10(8): 3052-3056
- [18] BOUARISSA N, BACHIRI R, CHARIFI Z. Electronic properties of Al<sub>x</sub>Ga<sub>1-x</sub>As<sub>y</sub>Sb<sub>1-y</sub> alloys lattice-matched to InAs [J]. Physica Status Solidi B, 2001, 226: 293–304.
- [19] MUNTYANU F M. Quantum oscillations of magnetoresistance and thermomagnetic power and the fermi surface of As–Sb alloys [J]. Physica Status Solidi B, 1986, 136: 749–756.
- [20] GITSU D V, GOLBAN I M, MAKEICHIK A I, MUNTYANU F M, ONU M I. The Thermopower and the thermomagnetic power in arsenic-antimony alloys at low temperature [J]. Physica Status Solidi B, 1980, 100: 401–406.
- [21] CAO Hua-zhen, ZHONG Yang, WU Lian-kui, ZHANG Yu-feng, ZHENG Guo-qu. Electrodeposition of As-Sb alloy from high arsenic-containing solutions [J]. Transactions of Nonferrous Metals

- Society of China, 2016, 26(1): 310-318.
- [22] LAJNEF M, EZZAOUIA H, CHTOUROU R. Optical characterization of InAs film grown on SnO<sub>2</sub> substrate by the electrodeposition technique [J]. Journal of Physics D: Applied Physics, 2008, 41(12): 125–302.
- [23] MOUANGA M, RICQ L, DOUGLADE J, BERCOT P. Corrosion behaviour of zinc deposits obtained under pulse current electrodeposition: Effects of coumarin as additive [J]. Corrosion Science, 2009, 51(3): 690–698.
- [24] SCHARIFKER B R, MOSTANY J. Three-dimensional nucleation with diffusion controlled growth. Part I: number density of active sites and nucleation rates per site [J]. Journal of Electroanalytical Chemistry, 1984, 177(1–2): 13–23.
- [25] SCHARIFKER B, HILLS G. Theoretical and experimental studies of multiple nucleation [J]. Electrochimica Acta, 1983, 28(7): 879–889.
- [26] HOLZLE M H, RETTER U, KOLB D M. The kinetics of structural changes in Cu adlayers on Au(111) [J]. Journal of Electroanalytical Chemistry, 1994, 371(1–2): 101–109.
- [27] MENTAR L, KHELLADI M R, AZIZI A, KAHOUL A. Effect of potential on the early stages of nucleation and growth during cobalt electrocrystallization in sulfate medium onto FTO surface [J]. Materials Letters, 2010, 64(21): 2403–2406.
- [28] DIAZ-MORALES O, MOSTANY J, BORRAS C, SCHARIFKER B R. Current transient study of the kinetics of nucleation and diffusion-controlled growth of bimetallic phases [J]. Journal of Solid State Electrochemistry, 2013, 17(2): 345–351.
- [29] CAO Hua-zhen, CHEN Jin-zhong, YUAN Hai-jun, ZHENG Guo-qu. Preparation of pure SbCl<sub>3</sub> from lead anode slime bearing high antimony and low silver [J]. Transactions of Nonferrous Metals Society of China, 2010, 20(12): 2397–2403.
- [30] CHEN Jin-zhong, CAO Hua-zhen, LI Bo, ZHENG Guo-qu. Thermodynamic analysis of separating lead and antimony in chloride system [J]. Transactions of Nonferrous Metals Society of China, 2009, 19(3): 730–734.
- [31] DENG Xue-rong, WANG Li-shi, ZHANG Shui-feng, LIU Xiao-xiao, MO Jin-yuan. Simultaneous determination of ascorbic acid and

- dopamine at electropolymerized manganese(III) 5-[o-(1-imidazole butoxy) phenyl]-10, 15, 20-triphenylporphrine chloride film-modified glass carbon electrode [J]. Chinese Journal of Analytical Chemistry, 2006, 34(5): 637–641.
- [32] LI W, LANE A M. Resolving the H<sub>UPD</sub> and H<sub>OPD</sub> by DEMS to determine the ECSA of Pt electrodes in PEM fuel cells [J]. Electrochemistry Communications, 2011, 13(9): 913–916.
- [33] JERKIEWICZ G. Hydrogen sorption at/in electrodes [J]. Progress in Surface Science, 1998, 57(2): 137–186.
- [34] CAO Hua-zhen, SHAN Han-peng, RUAN Hui-min, ZHENG Guo-qu. A study on the evolution of arsine during arsenic electrodeposition: The influence of ammonium citrate [J]. Electrochemistry Communications, 2012, 23: 44–47.
- [35] BEJAN D, BUNCE N J. Electrochemical reduction of As(III) and As(V) in acidic and basic solutions [J]. Journal of Applied Electrochemistry, 2003, 33(6): 483–489.
- [36] MENZIES I A, OWEN L W. The electrodeposition of arsenic from aqueous and non-aqueous solutions [J]. Electrochimica Acta, 1966, 11(2): 251–265.
- [37] WANG H, PRITZKER M. Effect of low concentrations of Pb<sup>2+</sup> on Sn electrodeposition in methyl sulphonic acid solutions [J]. Electrochimica Acta, 2008, 53(5): 2430–2440.
- [38] SOTO A B, ARCE E M, PALOMAR-PARDAVE M, GONZALEZ I. Electrochemical nucleation of cobalt onto glassy carbon electrode from ammonium chloride solutions [J]. Electrochimica Acta, 1996, 41(16): 2647–2655
- [39] VAZQUEZ-ARENAS J, CRUZ R, MENDOZA-HUIZAR L H. The role of temperature in copper electrocrystallization in ammoniachloride solutions [J]. Electrochimica Acta, 2006, 52(3): 892–903.
- [40] RADISIC A, LONG J G, HOFFMANN P M, SEARSON P C. Nucleation and growth of copper on TiN from pyrophosphate solution [J]. Journal of the Electrochemical Society, 2001, 148(1): C41-C46.
- [41] GRUJICIC D, PESIC B. Electrodeposition of copper: The nucleation mechanisms [J]. Electrochimica Acta, 2002, 47(18): 2901–2912.

# 盐酸体系中 As-Sb 合金的电结晶形核/生长机理

曹华珍,张煜峰,王倩倩,伍廉奎,郑国渠

浙江工业大学 材料科学与工程学院, 杭州 310014

摘 要:通过循环伏安(CV)测试和电流暂态曲线研究玻碳电极(GC)表面 As-Sb 合金的初期电结晶行为。绘制无因次电流暂态曲线,发现 As-Sb 合金的初期电结晶形核/生长过程遵循受扩散控制的三维形核模型。通过对电流暂态曲线分析计算得到相关形核参数。重点研究 Sb(III)浓度对形核过程的影响。定量分析结果表明,Sb(III)能加快As-Sb 合金的形核速度,从而使沉积物形貌由颗粒状结构转变为致密的层状结构。

关键词: 砷; 锑; As-Sb 合金; 电沉积; 形核

(Edited by Wei-ping CHEN)